Journal of Additive Manufacturing Technologies
DOI: 10.18416/JAMTECH.2212687

Infinite Science | Publishing

Coordination of spatial & temporal laser beam profile towards ultra-fine feature fabrication in laser powder bed fusion

A. Aktas[1, 2*], L. Caprio[1], F. Galbusera[1], B. Previtali[1], *and* A. G. Demir[1]

[1] Department of Mechanical Engineering, Politecnico di Milano, via La Masa 1, 20156 Milano, Italy
[*] Corresponding author, email: ali.aktas@polimi.it

Abstract

The Laser Powder Bed Fusion (LPBF) is a metal Additive Manufacturing (AM) technology, which uses high power laser beam and powder material to fabricate intricate geometries. Although LPBF theoretically offers high dimensional flexibility, the fabrication of thin (200-500µm) and ultra-thin (<200µm) features is still challenging due to geometrical fidelity and dimensional accuracy issues. This study addressed these challenges by assessing the fabrication capability of an LPBF systems while working with different dimension ranges in 2D. The study employed laser marking tests on the industrial LPBF system with open architecture to decompose errors related to scanning performance and process parameters during contour-hatch scanning via different laser emission modes. Additionally, the study provided linear parameters that connect the temporal and spatial domains, enabling scaling of the scanning vectors and optimization of spatial energy distribution during scanning with pulsed wave laser emission mode. The results showed that in the case of tuning the process parameters under system feasibility constrains, it is possible to achieve sufficient geometrical accuracy for scan trajectories. In this context, the study evaluated the inherent potential of LPBF systems in the fabrication of thin and ultra-thin features and provided a practical solution for achieving satisfactory geometrical accuracy.

Keywords: LPBF, dimensional feasibility, temporal-spatial laser beam control, geometrical fidelity, ultra-thin features

1. Introduction

Laser powder bed fusion (LPBF) is an advanced metal additive manufacturing technology that enables high shape and dimensional flexibility compared to traditional methods. It is possible to describe the process as a free-form manufacturing technique, making it ideal for applications requiring complex geometries and high performance. However, the fabrication of parts with ultra-fine geometrical features, such as wall thickness or strut size below 200 µm, remains a challenge for the technology [1]. This is because the geometrical fidelity of these features decreases when their dimensions become comparable to the laser beam diameter and the powder grain size, which are typically around 50-100 µm. As a result, the mismatch between the digital model and the final geometry is a significant obstacle to overcome. Studies on ultra-fine features in LPBF technology have typically focused on addressing the solution through process parameters and scanning strategies. The vast majority of the studies have emphasized the importance of using optimal process parameters and the correct scanning strategy to minimize the dimensional mismatch between the actual and final model [1]–[4]. Nevertheless, the technological limitations of LPBF machines with regard to temporal-spatial synchronization and laser beam control have been generally overlooked. Although some studies have investigated application feasibility in the parameter, geometry, and technology domains separately, these limitations, collectively known as scanning performance, have not been studied extensively [5]–[12]. On the other hand, despite there are mono-dimensional benchmark studies for LPBF system performance and feasibility, comprehensive results regarding scanning performance and related trajectory issues are still missing [13]–[15]. Moreover, well-defined process parameters and design rules for specific structures in the ultra-fine segment have been also presented in literature [16], [17]. However, the repeatability and validation of these studies are still contentious due to the variability in the technological capacity of LPBF machines.

Nevertheless, industrial-grade LPBF systems are developed primarily for producing larger dimensions and often do not operate at their full potential when it comes to producing fine features. These systems have scanner heads and fiber laser sources that are capable of greater spatial and temporal control on emission profiles, which are required for producing ultra-fine dimensions. However, due to rigid machine architectures, end-users hardly access parameters related to the scanner dynamics and laser temporal emission profile independently. This situation has limited the exploration of these systems' features. To develop the process towards ultra-fine features requires high parameter flexibility (such as custom laser delays). Moreover, some parameters related to the

scanner dynamics should be provided by the producers for optimizing different laser emission modes. Therefore, this study highlights the significance of detecting parameter-and-scanning-induced errors at the initial stage and decomposing them to accurately identify the processing capability and system precision at a 2D scan layer level before progressing towards complex 3D geometries with optimizing scanner and laser related parameters.

2. Modelling of the Emission Modes

Control of the laser source during different emission modes, as well as the difficulties involved, can theoretically be explained with mathematical concepts. Primarily, it is possible to indicate two main laser emission modes (laser modalities) used by LPBF machines during the conventional scanning (vectorial hatching strategy with moving laser beam). Specifically, the Continuous Wave (CW) emission provides a constant release of energy under constant scanning speed, while Pulsed Wave (PW) emission mode releases energy intermittently through fast power modulation (see Fig 1 A-C). In PW emission mode, pulse frequency (f_p) is defined by laser-on (t_{on}) and laser-off (t_{off}) times as follows, and it is a fundamental property of the laser power variations (see Fig 1A-B).

$$f_p = \frac{1}{t_{on} + t_{off}} \quad (1)$$

Duty cycle (δ) is the main relation for controlling pulse width in the time domain, and transition between PW and CW emission modes (Fig 1). It is possible to calculate it via the following equation.

$$\delta = \frac{t_{on}}{t_{on} + t_{off}} = t_{on} \cdot f_p \quad (2)$$

The laser emission mode is getting closer to CW with decreasing laser-off time (t_{off}). When the t_{off} becomes equal to zero, the duty cycle reaches to 1 (100%), and the laser emission mode transforms to the continuous mode (Fig 1C).

Although the square pulse shapes are using conceptually to explain the temporal behavior of the laser beam, the actual temporal behavior is different from the theoretical one. Hence, controlling spatial energy distribution becomes much more difficult during the scanning. As it can be seen from Fig 2A, in the case of actual temporal behavior, there is an initial ramp after the laser source is turned-on, power peak that is possible to described with fiber relaxation phenomena, regime condition which is the desired condition, and final ramp before going toward zero [18]. Therefore, while the theoretical pulse energy (E_{th}) can be calculated via using laser peak power in the case of perfect pulses (Fig 1A-B)(3)(4),

$$P_{pk} = \max_{0 < t < t_{on}} P(t) \quad (3)$$

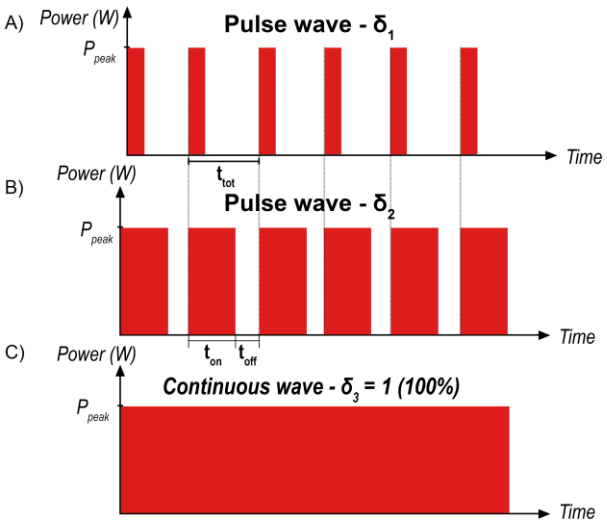

Fig 1. Theoretical temporal pulse shapes: Perfect temporal profiles. A) PW-low duty cycle with total pulse time (t_{tot}). B) PW-high duty cycle with laser-on (t_{on}) and laser-off (t_{off}) times. C) CW- with δ = 100%.

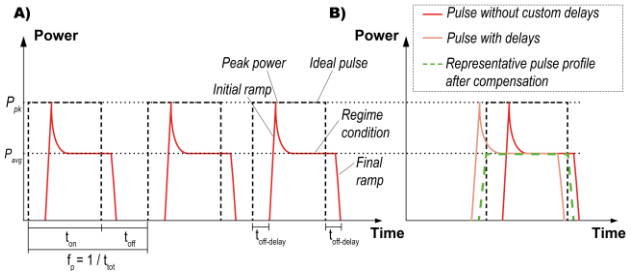

Fig 2. A) Real temporal shape of the laser beam. B) Temporal shape after time compensation: Laser custom delays, $t_{on\text{-}delay}$ & $t_{off\text{-}delay}$.

$$E_{th} = P_{pk} \cdot t_{on} \quad (4)$$

the actual pulse energy (E) should be calculated by using an averaged or time-variate pulse power. Considering the non-linear relation of the time and the pulse power (Fig. 2A), the manufacturers are measuring this relation experimentally during the total duration of a pulse and giving the average pulse power (P_{avg}) according to the pulse frequency (f_p) (5) [19],[20].

$$E = P_{avg} \cdot (t_{on} + t_{off}) \quad (5)$$

Based on the given formula (5), for lower time modulations during the scanning of ultra-thin regions on the powder bed, temporal-spatial synchronization with uniform spatial energy distribution becomes much more difficult. However, considering the thermal nature of the process, it is essential to provide uniform energy distribution to prevent failures and achieve better mechanical properties. Considering the asymmetric behavior of power over the pulse duration that can be associated with optoelectronic systems and laser control architectures, and the lower modulation times, using experimental methods for temporal-spatial calibration is a more effective approach to improving

scanning performance. Therefore, in the study, practical assessment of the laser source behavior was carried out experimentally and energy release manipulated by the custom laser delays for the better energy distribution on the powder bed.

Accordingly, two of most important custom laser delays, $t_{on\text{-}delay}$ & $t_{off\text{-}delay}$ were used for temporal optimization (Fig 2B). In addition of these two delays, other custom delays provided by the utilized LPBF system, such as jump delay, mark delay etc., were used to improve temporal-spatial coherence and enhance precision during the scanning, but these custom parameters were kept out of this study.

In LPBF machines, the laser sources use a mechanism called laser on-the-fly, which means that the laser source emits energy continuously according to the defined modality during the scanning process, regardless of spatial coordinates and scanning speed [21]. While CW laser modality requires less effort in terms of synchronization due to the continuous emission during the scanning, calibration should be performed considering intersection of the temporal and spatial domain for the PW laser modality due to the sustained modulation of the laser power. Therefore, the scanning speed and pulse duration were associated with a mathematical description, which provides intersection of temporal and spatial domains together. Considering the operation and control mechanism of the laser module, two mathematical relations were used to calibrate temporal-spatial behavior of the source. One of the employed parameters; laser-on distance (LOD) (Fig 3) is a sub-scanning vector, where the laser is operating, on a hatch vector along the scanning area (6).

$$LOD = \mathrm{v} \cdot t_{on} \quad (6)$$

On the contrary, laser-off distance (LFD) (Fig 3) is the sub-vector on a hatch vector where the laser source is not operating (7).

$$LFD = \mathrm{v} \cdot t_{off} \quad (7)$$

In the both equations (6) and(7) , v represents the scanning speed (mm/s).

The provided equations were used to optimize the scanning performance and control spatial energy distribution on the powder bed in PW emission mode. Nonetheless, it should be considered that the laser-on and laser-off durations can be controlled through pulse frequency (1) or duty cycle (2) and scanning speed (v) on the employed LPBF system. Using the two main parameters (i.e., scanning speed and duty cycle) together in modelling and calibration of PW emission mode provides a benefit for scaling the physical effect of the pulses in spatial manner.

Indeed, to achieve optimal temporal-spatial calibration and enhanced precision in conventional scanning

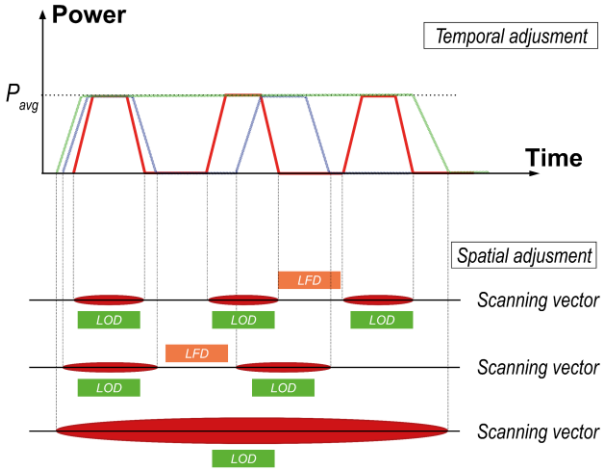

Fig 3. LOD and LFD demonstration over the scanning vectors for different scanning speeds and pulse durations.

methods, it is important to consider both the modulation frequency limit of a laser source and potential signal delays in electronic circuits. However, it is difficult to fulfill all these requirements due to the physical limits of the technology and number of parameters to achieve perfect synchronization.

3. Material and Methods

3.1. Material and Equipment

An industrial grade LPBF system with open architecture was used for the purpose of the study (LLA 150, 3DNT, Solbiate Olona, Italy). The laser emission could be controlled at a vector level allowing to operate the laser in continuous wave (CW), pulsed wave (PW) or single point exposure (SPE) flexibly with dedicated control software (Direct Machining Control, Vilnius, Lithuania). The machine operated with a single mode fiber laser (AFX1000, nLIGHT, Vancouver, WA, USA) coupled to a scanner head (MS-III, Raylase, Wessling, Germany). Moreover, the Al-5457 (designated as A95457 in UNS) was used as substrate during the marking tests. The substrates were polished and cleaned with alcohol to remove dirt and oxide layer from the surface before each marking test. Sample characterizations were made via optical microscope (EchoLAB® UM 300I BD), and the characterization results presented in the supplementary materials (A-D).

3.2. Study of Scanning feasibility and Optimization

The fixed and variable parameters for the experimental study are shown in Table 1 and Table 2.

Table 1. Fixed parameters for all the tests.

Spot size (µm)	Hatch distance (µm)	Shielding gas	Shielding gas (bar)	Laser-off time (µs)
47	30	Argon	0,5	50 (PW)

Table 2. Variable parameters for scanning performance analysis and optimization.

Test	Nominal radii, R_{nom} (µm)	Replicate	Duty cycle (%)	Laser power (W)	Scanning speed (mm/sec)	Laser-on delay (µs)	Laser-off delay (µs)	Explanation
1) CW: P-S	90; 180	2	100	[75:200] with 25W increment	[200-900] with 100 increment - additional: 1200;1400; 1600	- 90	+95	Observation of scanning capability under different parameter conditions
2) CW: S-R_{nom}	90; 100; 200; 300; 400; 500	1	100	200	[25:1500] with 25 mm/s increment	- 90	+95	Feasibility study; CW scanning performance investigation for various scanning speeds and nominal radii under fixed laser power condition
3) PW: P-S-DC	90; 180	2	[30 :80] with 10% increment	100;150; 200	200; 400; 800; 1600	- 90	+95	Physical observation of LOD that can be adjusted through duty cycle and scanning speed
4) Custom delays	Square shape	1	100	100; 150; 200	140; 500	0; -20; -80; -120	+20; +40; +60; +80	Optimization of the temporal behavior of the laser via custom delays and process parameters
5) PW: LOD-Vdn	90	1	20; 30; 40; 50	100;150;200; 250	75; 125; 175	-120	+80	Feasibility study; PW scanning performance investigation through LOD

Microscope observations are tabulated and given in supplementary materials(A-D). Regarding the negative sign in the laser-on delay in Table 2, it indicates that the laser switch-on command is issued prior to the movement of the laser beam. A positive value for the laser-off delay parameter indicates that the laser is switched off after the scanning action finishes.

For the characterization of the samples, total error (E_{tot}) wasemployed as sum of scanning (E_{scan}) and process ($E_{process}$) induced errors as following

$$E_{tot} = E_{scan} + E_{process} \quad (8)$$

The scan induced error (E_{scan}) was a result of an incorrect laser beam trajectory caused by the scanner's performance while the process induced error was associated with the selected process parameters ($E_{process}$) and thermal nature of the process (Fig 4). Furthermore, the numerical error (E_n), which includes both contributions (i.e., scan-and-process-induced errors), was calculated as the difference between the nominal radius (R_{nom}) and the measured radius (R_{meas}).

$$E_n = R_{nom} - R_{meas} \quad (9)$$

Moreover, to compare different nominal radii, it was employed a percentage-based approach using the absolute error (E_{abs} (%)) equation presented below.

$$E_{abs}(\%) = \frac{|R_{nom} - R_{meas}|}{R_{nom}} . 100 \quad (10)$$

Considering the scanning area, perimeter (contour part), and scanning speed, laser-material interaction time (t_{int}) was described in the following equation.

$$t_{int} = \frac{\frac{\pi R_{nom}^2}{d_h} + 2\pi R_{nom}}{v} \quad (11)$$

In the equation, d_h represents the hatch distance (distance between two scanning vector).

Nevertheless, during the characterization, sample measurements were taken from the outermost parts of the contours (Fig 5B) for considering error separation strategy. However, the study did not take into account beam compensation, which is a strategy used to compensate for laser beam divergence and achieve a desired spot size or beam profile at the target location (Fig 5A) [22]. Test sequences in Table 2, were arranged considering the specific requirements of the laser emission modes. Considering the interaction between the laser and scan-related parameters that could affect the outcome of the experiments, the tests separately assessed technological feasibility, optimum laser parameters for scanning performance, and the parameter interactions. At the final stage, the validation test was carried out to show effectiveness of the LOD/LFD parameters for process design.

Infinite Science | Publishing

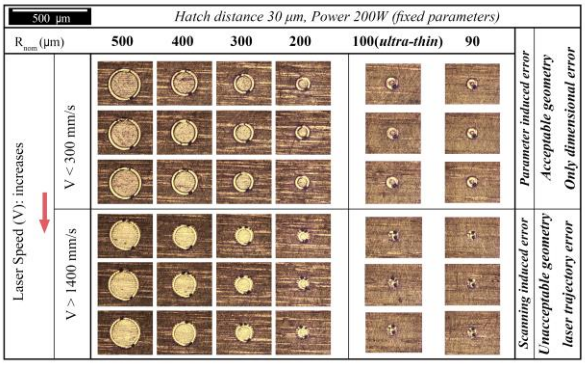

Fig 4. CW laser emission mode: Scan and parameter induced errors for different nominal radii.

4. Results and Discussion

The preliminary test, Test 1 in Table 2, was addressed to check scanner behavior under different processing conditions. The actual and nominal radii along with the processing conditions are shown in Fig 6. The scatter plot indicates that the values lower than nominal radii is possibly associated with the scanning error due to the thermal nature of the process. This means that higher actual radii should be expected in cases where the level of parameter-induced errors is high due to higher energy deposition. Additionally, the scanning error is more evident for the nominal radius of 180 µm at higher scanning speeds (v), while it is less noticeable for the nominal radius of 90 µm. This is because the small scanning area of 90 µm is not sufficient to reflect the error numerically even though the damages are clearly seen on the optical microscope observations (Fig 4).

To assess technological feasibility, the second test was conducted under a fixed laser power condition for various scanning speeds and nominal radii. As shown in Fig 7, the error data for the ultra-thin (<200µm) and near ultra-thin (300µm) segments follows a 'V' shape distribution, whereas a more flattened error distribution is observed for larger nominal radii. This type of data distribution is indicative of scan-induced and parameter-induced errors, which can be attributed to the critical interaction time. For the interaction times that are lower than the critical one, the error is highly correlated to the galvo scanner performance. On the other hand, the error trend becomes more stable and numerically lower for interaction times higher than the critical one. Furthermore, as shown in Fig 8, for radii greater than 300 µm, the error trend decreases with increasing scanning speed under fixed laser power condition, resulting in a more flattened trend due to the decreasing linear energy density.

Indeed, the relationship between scanning speed and error trends can vary depending on specific circumstances and factors. In the case of the tests performed under fixed power conditions, an increase in scanning speed leads to lower thermal energy deposition. Consequently, a reduction in process-induced errors is expected due to the reduced thermal energy. Therefore, in the case of absence or reduction of the scan-induced error, the total error described in equations (8) and (9), should decrease with an increase in scanning speed.

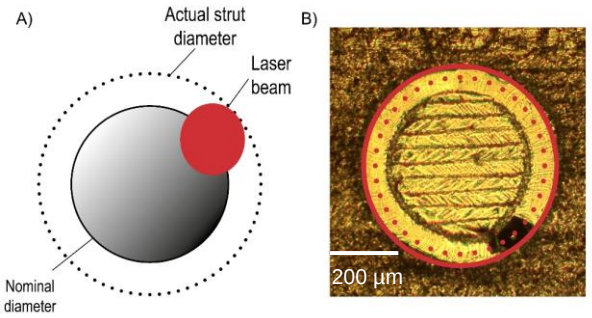

Fig 5. A) Nominal and actual diameter representative illustration (contribution of the laser beam to final strut diameter). B) The measurement procedure (dashed line is laser beam path, continuous line is measured path).

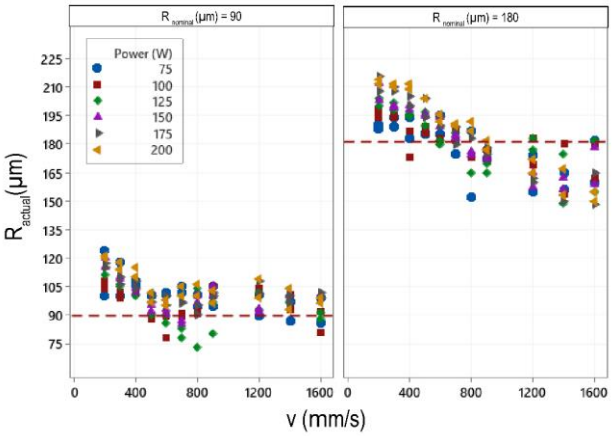

Fig 6. Scatter plot - Test 1: 90 and 180 µm nominal radii vs. actual radii under different processing conditions.

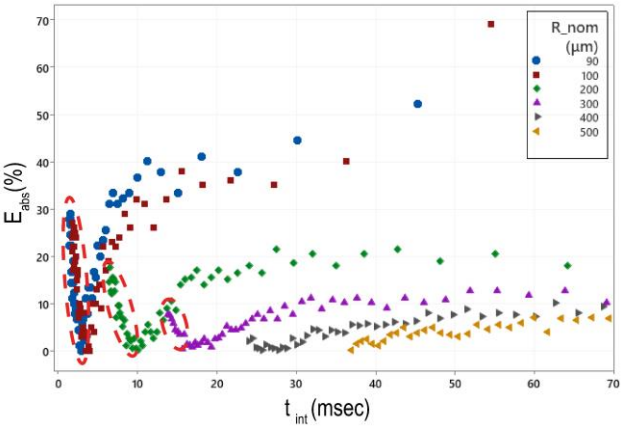

Fig 7. Test 2: Critical interaction time for error separation: Scanning induced error region is inside the dashed red circles.

On the contrary, for ultra-thin and near ultra-thin dimensions, the error trend started to increase after 1000 mm/s with increasing scanning speed (Fig 8). In this context, the unexpected data behavior in Fig 8 was attributed to scanning-induced errors caused by reduced scanning precision due to the high scanning speeds. Considering the error trend and scanning speeds, region II (600-1000 mm/s) appears to be the most feasible for the fabrication, from a technological standpoint. This region may provide the balance between scanning speed and precision, leading to a lower error trend and higher accuracy in the final product in the case of optimum laser power conditions.

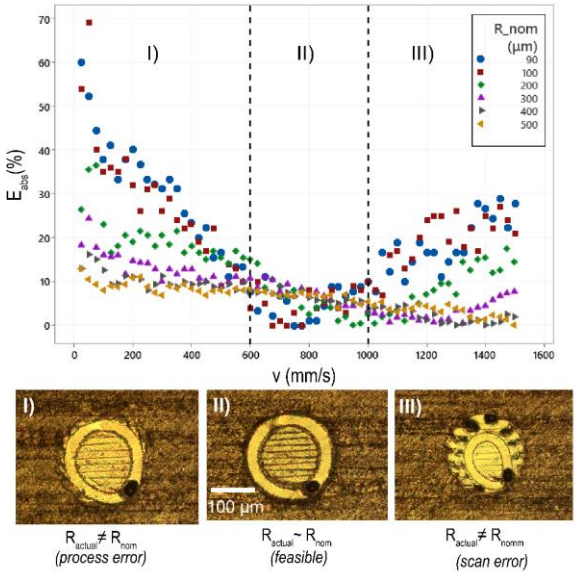

Fig 8. Scatter plot – Test 2: Absolute error (%) vs. scanning speed time for different nominal radii.

Based on the analysis of the characterized samples, a limit scanning speed was identified for each nominal radius beyond which the hatching vectors begin to pass over the contour part of the geometry (Supplementary Material-B). Accordingly, scanning speeds over the limit for each nominal radius might be associated with the surface roughness issues on the final product in actual fabrication process.

Nevertheless, Fig 9A shows the physical effects of the duty cycle and scanning speed as a result of the Test 3 (Table 2). The test was performed to address the LOD/LFD parameters before calibration process during PW laser modality. As highlighted in Fig 9A, when the duty cycle was high (greater than 50%), longer scan tracks were observed as a result of the laser on-the-fly mechanism and higher laser-on time. Additionally, thermal damages on the scanning area clearly showed the effects of unoptimized custom laser delays and high LOD with improper laser power during the pulse sequences of the PW modality. Correspondingly, the preliminary feasibility region for LOD/LFD and the effect of laser parameters were physically shown as a result of this test. Considering the interaction of the laser parameters on scanning performance, an optimization test was carried out for the laser custom delays before the last test (Test 5).

Additionally, Fig 9B illustrates the laser custom delay optimization process through three representative images (Test 4). The test highlight the potential damage on the contour-hatch junction points that may result from improper setting of laser custom delays. Such damages occur because the laser turn-on-and-off commands are sent at the beginning and end of each hatch vector, and improper delays can lead to a lack of fusion or thermal damage at hatch-contour junction points. Therefore, it is essential to optimize these delays by considering the interaction between the process parameters. With the feasible delays, observed damages on the junction points as well as at the end of the pulses in PW laser modality might be compensated

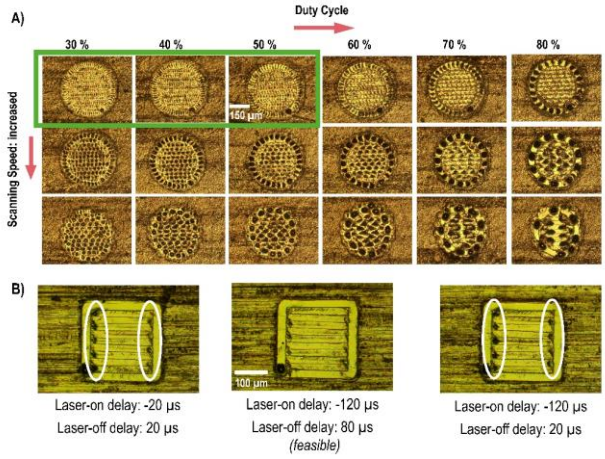

Fig 9. PW laser emission: Scanning performance investigation study: A) Test 3-Investigation on LOD and LFD (green rectangle-optimal region), B) Test 4-Laser custom delays.

for, resulting in a more accurate geometrical shape and more precise scanning overall. Therefore, for the next test, the laser-on delay and laser-off delay were selected as -120 µs and +80 µs, respectively.

For validation of the findings in Test 3 and Test 4, the Test 5 was performed. Based on the limitations in the scanning process for PW laser modality (Test 3), lower scanning speeds and duty cycles were found to result in better temporal-spatial control and energy distribution over the scanning area. Therefore, it was focus on the experimental area where the duty cycle was below 50% with low scanning speeds, in order to achieve a lower LOD. The results validated the findings in previous tests. The use of LOD for the optimization, along with proper laser custom delays and optimum power conditions, resulted in better scanning performance (Supplementary Material-D).

5. Conclusions

Scanning performance of the LPBF system and possible optimization with calibration were evaluated in terms of fine and ultra-fine features. The errors caused by the process parameters and scanner performance were practically shown. Additionally, technological feasibility of the employed LPBF system was defined, and an investigation methodology for the industrial machines was provided. In this perspective, laser marking tests aided to define the feasibility ranges for the different feature sizes (90-500 µm radii) were employed. The link between the scanning speed and the minimum vector length for a stable laser emission profile was established for PW laser modality. The study found that scanning trajectories based on conventional hatching methods can achieve with sufficient geometrical accuracy if the correct scanning parameters are selected within the technological feasibility window. In this context, it was emphasized that the technology involves a trade-off between dimension flexibility and system capability. Thus, the theoretical manufacturing capacity (i.e., free-form manufacturing) is primarily constrained by the system's technological feasibility, rather than process parameters or scanning strategies.

Furthermore, it should be noted that the effectiveness of numerical error indicators (8) and (9) are highly dependent on the geometry and dimensional range being characterized. As a result, these indicators may be inadequate for defining the actual errors caused by scanner systems, particularly in the ultra-fine dimensional range. Although scanning errors are clearly visible in optical microscopy images, numerical errors may not always provide accurate results. Therefore, using time-based formulation may be more suitable for detection. In this sense, the study provided a time-based formula that shows the critical interaction time for the separation of scanning-induced and parameter-induced errors. According to the provided formula, it is possible to limit the scanning speed, considering the scanning area and perimeter (contour) as independent from the geometry, in order to reduce geometrical fidelity problems.

Acknowledgments

Optoprim® and nLight® are acknowledged for providing the laser source. The authors would like to thank also DMC for the support in the development of the software architecture and Raylase for the longstanding collaboration. This work has been supported by the National Plan for Recovery and Resilience (PNRR).

Author's statement

Conflict of interest: Authors state no conflict of interest. Informed consent: Informed consent has been obtained from all individuals included in this study. Ethical approval is not required.

References

[1] O. Rehme and C. Emmelmann, "Rapid manufacturing of lattice structures with Selective Laser Melting," in Lasers in Manufacturing, 2006, vol. 6107. doi: 10.1117/12.645848.

[2] E. Abele, H. A. Stoffregen, K. Klimkeit, H. Hoche, and M. Oechsner, "Optimisation of process parameters for lattice structures," Rapid Prototyp. J., vol. 21, no. 1, pp. 117–127, 2015, doi: 10.1108/RPJ-10-2012-0096.

[3] R. Vrána et al., "Selective laser melting strategy for fabrication of thin struts usable in lattice structures," Materials (Basel)., vol. 11, no. 9, 2018, doi: 10.3390/ma11091763.

[4] A. du Plessis et al., "Properties and applications of additively manufactured metallic cellular materials: A review," Prog. Mater. Sci., vol. 125, no. April 2021, p. 100918, 2022, doi: 10.1016/j.pmatsci.2021.100918.

[5] D. Wang, S. Wu, Y. Bai, H. Lin, Y. Yang, and C. Song, "Characteristics of typical geometrical features shaped by selective laser melting," J. Laser Appl., vol. 29, no. 2, p. 022007, 2017, doi: 10.2351/1.4980164.

[6] J. Kranz, D. Herzog, and C. Emmelmann, "Design guidelines for laser additive manufacturing of lightweight structures in TiAl6V4," J. Laser Appl., vol. 27, no. S1, p. S14001, 2015, doi: 10.2351/1.4885235.

[7] A. G. Demir, P. Colombo, and B. Previtali, "From pulsed to continuous wave emission in SLM with contemporary fiber laser sources: effect of temporal and spatial pulse overlap in part quality," Int. J. Adv. Manuf. Technol., vol. 91, no. 5–8, pp. 2701–2714, Jul. 2017, doi: 10.1007/s00170-016-9948-7.

[8] L. Caprio, A. G. Demir, and B. Previtali, "Comparative study between CW and PW emissions in selective laser melting," J. Laser Appl., vol. 30, no. 3, p. 032305, Aug. 2018, doi: 10.2351/1.5040631.

[9] L. Caprio, A. G. Demir, and B. Previtali, "Influence of pulsed and continuous wave emission on melting efficiency in selective laser melting," J. Mater. Process. Technol., vol. 266, no. September 2018, pp. 429–441, 2019, doi: 10.1016/j.jmatprotec.2018.11.019.

[10] F. Guaglione, L. Caprio, B. Previtali, and A. G. Demir, "Single point exposure LPBF for the production of biodegradable Zn-alloy lattice structures," Addit. Manuf., vol. 48, no. June, 2021, doi: 10.1016/ j.addma. 2021. 102426.

[11] K. Gunaydin, H. S. Türkmen, A. Airoldi, M. Grasso, G. Sala, and A. M. Grande, "Compression Behavior of EBM Printed Auxetic Chiral Structures," Materials (Basel)., vol. 15, no. 4, pp. 1–21, 2022, doi: 10.3390/ma15041520.

[12] O. Gülcan and K. Günaydın, "Distortion and dimensional deviation of Inconel 718 auxetic structures produced by DMLM," J. Addit. Manuf. Technol., doi: 10.18416/ JAMTECH.2111563.

[13] M. Moshiri, S. Candeo, S. Carmignato, S. Mohanty, and G. Tosello, "Benchmarking of laser powder bed fusion machines," J. Manuf. Mater. Process., vol. 3, no. 4, 2019, doi: 10.3390/jmmp3040085.

[14] J. Kruth, B. Vandenbroucke, J. Van Vaerenbergh, and P. Mercelis, "Benchmarking of different SLS / SLM processes as rapid manufacturing techniques," 2005.

[15] B. Vandenbroucke and J. P. Kruth, "Selective laser melting of biocompatible metals for rapid manufacturing of medical parts," Rapid Prototyp. J., vol. 13, no. 4, pp. 196–203, 2007, doi: 10.1108/13552540710776142.

[16] L. L. Lopez Taborda, H. Maury, and J. Pacheco, "Design for additive manufacturing: a comprehensive review of the tendencies and limitations of methodologies," Rapid Prototyp. J., no. April 2020, 2021, doi: 10.1108/RPJ-11-2019-0296.

[17] M. K. Thompson et al., "Design for Additive Manufacturing: Trends, opportunities, considerations, and constraints," CIRP Ann. - Manuf. Technol., vol. 65, no. 2, pp. 737–760, 2016, doi: 10.1016/j.cirp.2016.05.004.

[18] A. G. Demir, B. Previtali, and N. Lecis, "Development of laser dimpling strategies on TiN coatings for tribological applications with a highly energetic Q-switched fibre laser," Opt. Laser Technol., vol. 54, pp. 53–61, 2013, doi: 10.1016/j.optlastec.2013.05.007.

[19] W. M. Steen and J. Mazumder, "Background to Laser Design and General Applications," Laser Mater. Process., pp. 11–78, 2010, doi: 10.1007/978-1-84996-062-5_2.

[20] W. M. Steen, "'Light' industry: An introduction to laser processing and its industrial applications," Adv. Laser Mater. Process. Technol. Res. Appl., pp. 3–19, 2010, doi: 10.1533/9781845699819.1.3.

[21] M. Stoesslein, D. Axinte, and D. Gilbert, "On-The-Fly Laser Machining: A Case Study for in Situ Balancing of Rotative Parts," J. Manuf. Sci. Eng. Trans. ASME, vol. 139, no. 3, 2017, doi: 10.1115/1.4034476.

[22] M. Moesen, T. Craeghs, J. P. Kruth, and J. Schrooten, "Robust beam compensation for laser-based additive manufacturing," CAD Comput. Aided Des., vol. 43, no. 8, pp. 876–888, 2011, doi: 10.1016/j.cad.2011.03.004.